CrossMark

iPTF Archival Search for Fast Optical Transients

Anna Y. Q. Ho[1] , S. R. Kulkarni[1] , Peter E. Nugent[2] , Weijie Zhao[3], Florin Rusu[3], S. Bradley Cenko[4,5] , Vikram Ravi[1] ,
Mansi M. Kasliwal[1] , Daniel A. Perley[6] , Scott M. Adams[1], Eric C. Bellm[7], Patrick Brady[8], Christoffer Fremling[1] ,
Avishay Gal-Yam[9] , David Alexander Kann[10] , David Kaplan[8] , Russ R. Laher[11] , Frank Masci[11] , Eran O. Ofek[9] ,
Jesper Sollerman[12] , and Alex Urban[13]

[1] Cahill Center for Astrophysics, California Institute of Technology, MC 249-17, 1200 East California Boulevard, Pasadena, CA 91125, USA; ah@astro.caltech.edu
[2] Lawrence Berkeley National Laboratory, 1 Cyclotron Road, Berkeley, CA 94720, USA
[3] University of California Merced, 5200 Lake Road, Merced, CA 95340, USA
[4] Astrophysics Science Division, NASA Goddard Space Flight Center, Mail Code 661, Greenbelt, MD 20771, USA
[5] Joint Space-Science Institute, University of Maryland, College Park, MD 20742, USA
[6] Astrophysics Research Institute, Liverpool John Moores University, IC2, Liverpool Science Park, 146 Browlow Hill, Liverpool L3 5RF, UK
[7] University of Washington Astronomy Dept., Box 351580, Seattle, WA 98195, USA
[8] Department of Physics, University of Wisconsin-Milwaukee, Milwaukee, WI 53201, USA
[9] Benoziyo Center for Astrophysics, Weizmann Institute of Science, 76100 Rehovot, Israel
[10] Instituto de Astrofísica de Andalucía (IAA-CSIC), Glorieta de la Astronomía s/n, E-18008 Granada, Spain
[11] Infrared Processing and Analysis Center, California Institute of Technology, Pasadena, CA 91125, USA
[12] Department of Astronomy and The Oskar Klein Centre, AlbaNova University Center, Stockholm University, SE-106 91 Stockholm, Sweden
[13] LIGO Laboratory, California Institute of Technology, Pasadena, CA 91125, USA

Abstract

There has been speculation about a class of relativistic explosions with an initial Lorentz factor Γ_{init} smaller than that of classical gamma-ray bursts (GRBs). These "dirty fireballs" would lack prompt GRB emission but could be pursued via their optical afterglow, appearing as transients that fade overnight. Here we report a search for such transients (that fade by 5-σ in magnitude overnight) in four years of archival photometric data from the intermediate Palomar Transient Factory (iPTF). Our search criteria yielded 50 candidates. Of these, two were afterglows to GRBs that had been found in dedicated follow-up observations to triggers from the *Fermi* GRB Monitor. Another (iPTF14yb) was a GRB afterglow discovered serendipitously. Eight were spurious artifacts of reference image subtraction, and one was an asteroid. The remaining 38 candidates have red stellar counterparts in external catalogs. The photometric and spectroscopic properties of the counterparts identify these transients as strong flares from M dwarfs of spectral type M3–M7 at distances of $d \approx 0.15$–2.1 kpc; three counterparts were already spectroscopically classified as late-type M stars. With iPTF14yb as the only confirmed relativistic outflow discovered independently of a high-energy trigger, we constrain the all-sky rate of transients that peak at $m = 18$ and fade by $\Delta m = 2$ mag in $\Delta t = 3$ hr to be $680\ \mathrm{yr^{-1}}$, with a 68% confidence interval of 119–2236 $\mathrm{yr^{-1}}$. This implies that the rate of visible dirty fireballs is at most comparable to that of the known population of long-duration GRBs.

Key words: catalogs – gamma-ray burst: general – stars: activity – stars: flare – stars: jets – surveys

1. Introduction

The focus of this Letter is fast (significant fading in $\lesssim 1$ night) optical transients. The sky is poorly characterized on these timescales, in part because a short cadence comes at the cost of a decrease in sky coverage. These difficulties are exacerbated by the need for rapid follow-up. By contrast, novae and supernovae (SNe) evolve on timescales of days to weeks. It is therefore not surprising that they are the best-characterized classes of transients in the optical sky.

The dominant population of fast optical transients (FOTs) is flares from Galactic low-mass main sequence stars, particularly M dwarfs (e.g., Kulkarni & Rau 2006; Rau et al. 2008; Berger et al. 2013). These flares are thought to arise from magnetic reconnection events in convective envelopes. Behind this foreground of stellar flares is a population of extragalactic relativistic explosions: the optical afterglows to gamma-ray bursts (GRBs).[14] GRBs can be explained by the "collapsar" model: a star of mass

$M > 30\,M_\odot$ collapses to form a black hole, and the resulting accretion disk powers a jet (Piran 2004). The burst of γ rays arises from within the jet, while the optical afterglow is synchrotron emission from the jet shocking the circumstellar medium.

Searching for optical or radio afterglows could yield relativistic explosions that are related to GRBs but lack high-energy emission. One example is the hypothesized class of dirty fireballs (Dermer et al. 2000): explosions with a lower Γ_{init} than those of classical GRBs but with similar E_{iso} (energy released per unit solid angle). Classical GRBs are "clean" in the sense that they have a very low baryon loading fraction, which enables matter to be accelerated to hyper-relativistic (initial Lorentz factor $\Gamma_{init} \gtrsim 100$) speeds. The primary motivation to consider dirty fireballs is the absence of a compelling reason for all relativistic explosions to have the requisite low baryon loading. The prompt emission from a dirty fireball would peak at energies below the range of γ-ray detectors. However, like a classical GRB, a dirty fireball would produce a rapidly fading (on-axis) optical afterglow and long-lived radio emission (Rhoads 2003).

Another class of optical afterglows that would lack prompt high-energy emission are off-axis ("orphan") afterglows (Rhoads 1997). Unlike for classical (on-axis, $\theta_{obs} \lesssim 1/\Gamma_{init}$) GRBs, the observer of an off-axis burst would see neither the

---

[14] In this Letter we focus on transients related to long-duration GRBs because —due to their higher energetics and larger volumetric rates—these events dominate the observed population of relativistic explosions. However, short GRB afterglows also produce FOTs that could conceivably pass our selection criteria.

prompt high-energy emission nor the initial afterglow. However, as the jet slows down it also expands sideways, and as a result the afterglow becomes visible to an off-axis observer. While classical GRBs can be seen across the Universe due to relativistic beaming and Doppler boosting, orphan afterglows would be seen to shorter distances. However, the larger opening angle means that the solid angle of visibility is significantly larger than that of on-axis bursts (Nakar et al. 2002; Ghirlanda et al. 2015).

Wide-field optical surveys have already demonstrated the technical capability to find optical afterglows independently of a GRB trigger. For example, iPTF14yb (Cenko et al. 2015) and ATLAS17aeu (Bhalerao et al. 2017; Stalder et al. 2017) were optical afterglows to GRBs identified via fading broadband afterglow emission; in both cases, the "parent" GRB was identified only later (ibid). Then there is the curious PTF11agg (Cenko et al. 2013), which had no identified high-energy counterpart but had other characteristic features of a GRB afterglow: a rapidly fading optical source, a long-lived scintillating radio counterpart, and coincidence with a dwarf galaxy with an estimated redshift of $0.5 \lesssim z \lesssim 3.0$.

In this Letter, we report a search for FOTs in the *intermediate* Palomar Transient Factory (iPTF). This is similar to the search by Berger et al. (2013) for "fast optical transients" (defined as transients on timescales of 0.5 hr to 1 day) in 1.5 years of data from the Pan-STARRS-1 Medium Deep Survey (PS1/MDS). Relative to our search PS-1 is deeper (10σ of 22.5 mag in the equivalent of g and r bands). They found 19 transients; of these, eight were most reasonably explained as main-belt asteroids at their turning points, and the remaining 11 were linked with quiescent M-dwarf counterparts. This work emphasized the importance of avoiding low ecliptic latitudes for future searches, and highlighted the significant foreground of M-dwarf flares.

By focusing on fast transients, our search is sensitive to on-axis sources (dirty fireballs) and not off-axis events (orphan afterglows). The latter will be investigated in subsequent work, in which we search for transients that evolve rapidly on a timescale of days, like those in Drout et al. (2014) and Yang et al. (2017). Section 2 describes the survey, data, and search procedure, and Section 3 outlines the properties of the iPTF FOTs. In Section 4 we use the results of our search to constrain the rate of extragalactic FOTs. We conclude with a view to the upcoming Zwicky Transient Facility (ZTF; Bellm & Kulkarni 2017).

2. Data and Candidate Selection

The iPTF ran from 2013 January 1 to 2017 March 2 as the successor to the Palomar Transient Factory (PTF; Law et al. 2009). iPTF used a camera with a 7.26 deg^2 field of view on the 48 inch Samuel Oschin Schmidt Telescope at Palomar Observatory (P48) and a real-time image subtraction pipeline (Cao et al. 2016) run at the National Energy Research Scientific Computing Center (NERSC) to search for transient and variable activity in the night sky. The iPTF transient surveys generally emphasized higher-cadence observations than the PTF surveys, making them well-suited for searches for fast-fading events.

The full set of candidates were saved in a database at NERSC, and the subset that passed human inspection were saved in the iPTF database at Caltech. Light curves could also be obtained using the PTF IPAC/iPTF Discovery Engine (PTFIDE) tool (Masci et al. 2017), although PTFIDE has only been run on a small subset of the iPTF database due to computational expense.

Significant improvements to the image differencing pipeline (see Section 2) were made on 2013 February 1. We therefore selected this as the start date for our search. We then performed our search in four steps, listed below. The motivation for (a) and (c) is that the afterglows discovered by optical surveys thus far manifest themselves as sources that fade overnight: iPTF14yb faded by $\sim$0.7 mag/hr, ATLAS17aeu faded by $\sim$0.7 mag/hr, and PTF11agg faded by $\sim$0.2 mag/hr. With an initial magnitude of $r = 18$ mag, all three of these sources would become undetectable by iPTF (typical limiting mag $r \sim 20.5$ mag) within a night (14 hr, or 0.6 days). We chose to search for sources that have at least one pair of fading detections in order to accommodate the diversity of observed afterglow light curve shapes (e.g., Kann et al. 2010).

1. Query the NERSC database for candidates that have two detections[15] with magnitudes m_1, m_2 separated by Δt. This pair must satisfy the following criteria:
   (a) Fading ($m_2 > m_1$) within $\Delta t < 1$ night (0.6 day)
   (b) Real-bogus (RB[16]) score $\geqslant$0.3
   (c) All detections confined to 1 night (0.6 day)[17]
   (d) All detections spatially coincident to within $1{.}''5$
   (e) No bad image or bad subtraction flags (image_id > -1, sub_flag $\neq 0$)
2. Save all candidates from (1) to the iPTF database of named transients at Caltech. Many of these candidates were not in the iPTF database because they were not saved by human scanners (for example, because they fell below the RB threshold used during the survey).
3. Search the iPTF database (existing named transients as well as the ones added in Step [2]) for candidates exhibiting afterglow behavior: significant fading, $m_2 > m_1$ at 5-σ.
4. For all candidates in Step (3), generate forced PSF photometry on the difference image using PTFIDE to confirm the significance of the fading.

Of the 14,961 sources with a pair of detections separated by $\Delta t < 0.6$ days, there were 1371 sources with no detections outside of this window. Of these non-repeating sources, there were 680 sources that were fading. Of these 680 sources, there were 50 that had significant (5-σ) fading.

Of the candidates, one has two detections arising from two separate asteroids[18] and eight are artifacts of image subtraction identified in visual inspection. Note that the rate of false positives is what one would expect from the raw classifier performance (Bloom et al. 2012). Removing the asteroids and artifacts, we have 41 candidates. In Figure 1 we show the $\Delta t = t_{\rm end} - t_{\rm start}$ and $\Delta m = m_{\rm end} - m_{\rm start}$ for these 41 candidates. For reference, we show PTF11agg as well as a sample of GRB afterglows from the literature (Kann et al. 2010) sampled between three hours and nine hours after peak. iPTF14cva and iPTF14cyb were afterglows discovered by PTF in searches of the *Fermi* GBM error regions (Singer et al. 2015); they correspond to the events GRB 140620A (Kasliwal et al. 2014) and GRB 140623A (von Kienlin 2014), respectively. Note that there were six more afterglows detected by iPTF in follow-up *Fermi* GBM triggers (Singer et al. 2015), but these did not pass

---

[15] If there are >2 detections, there must exist a pair of detections satisfying (a) and (b).
[16] Brink et al. (2013).
[17] This eliminates periodic or repeating sources such as active galactic nuclei (AGN) and variable stars.
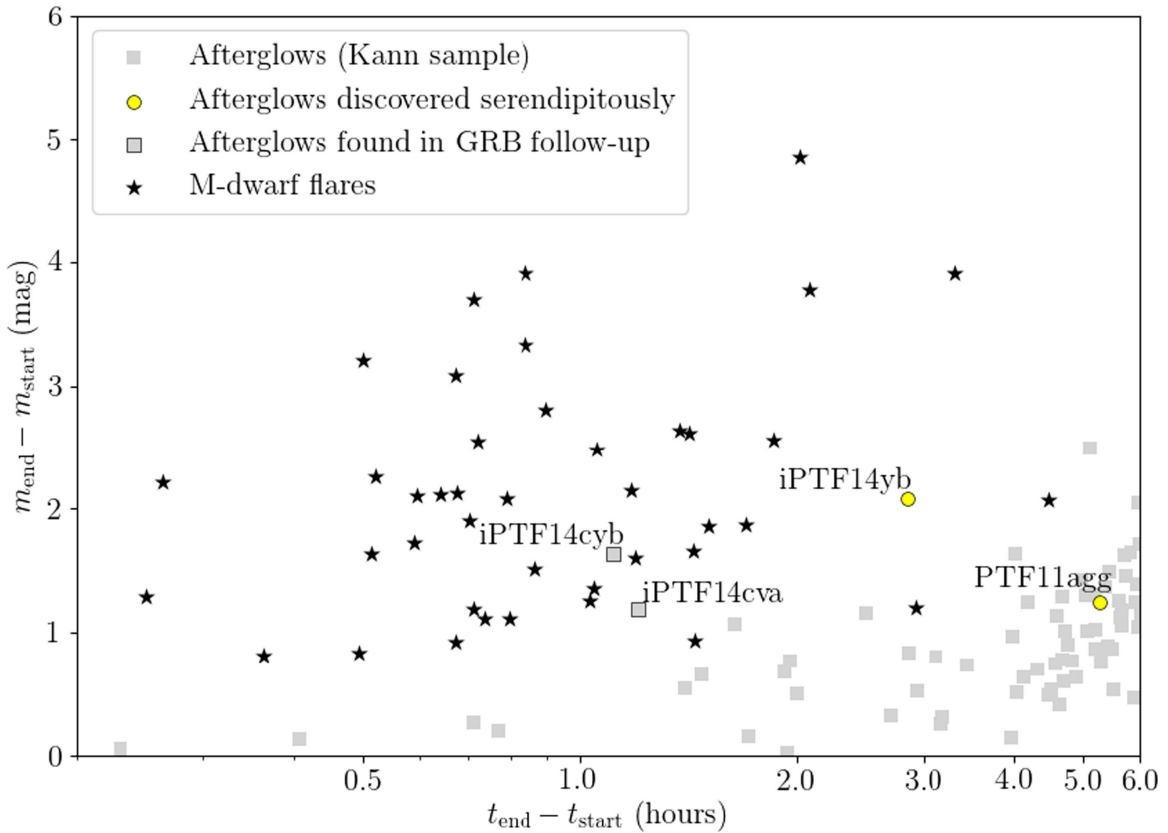[18] https://www.minorplanetcenter.net/cgi-bin/checkmp.cgi

Figure 1. $(\Delta t, \Delta m)$ for the 41 candidates that show significant (5-σ) intra-night fading (asteroids and artifacts of bad subtractions have been removed). The gray unlabeled points are a sample of GRB afterglows from Kann et al. (2010). For candidates with >2 points in their light curves, we show the change in magnitude from the first observation after 3 hr to the last observation before 9 hr (times measured since the burst): $\Delta t = t_{end} - t_{start}$ and $\Delta m = m_{end} - m_{start}$. M-dwarf flares typically fade faster and are detected in Pan-STARRS (see Table 1) with a characteristic red color. Thus, in our sample, filtering out sources with red hosts exclusively identifies iPTF14yb, the GRB discovered serendipitously by iPTF, as well as two afterglows found in follow-up to *Fermi* GRB triggers. PTF11agg is shown for reference. There is one M-dwarf with a Δt below the lower limit on the plot.

the search criteria because they were detected late after the trigger time and thus were not fading significantly (all below 5-σ).

The remaining 38 have red stellar hosts in external catalogs and can thus be identified as M-dwarf flares; we spectroscopically confirm these and discuss their properties in Section 3. Fortunately, all of the M dwarfs in our sample have red counterparts in external catalogs (described in Section 3), whereas none of the afterglows have detectable hosts. Indeed, of the 16 M-dwarf flares that were saved to the iPTF database during the survey (that is, prior to our search) 12 had red stellar counterparts in SDSS. The transients were thus readily classified as M-dwarf flares, although one was assigned for spectroscopic follow-up due to being faint ($r = 23.4$ mag). The full list of FOTs (ID, position, discovery date, and classification) can be found in Table 2.

3. Properties of the iPTF M-dwarf Flares

Figure 2 shows the light curves of all 38 M-dwarf flares, superimposed with the two afterglows discovered in survey mode (as opposed to in follow-up to GRBs). The positions and classifications can be found in Appendix A (Table 2).

For each candidate, a counterpart was present in the Panoramic Survey Telescope and Rapid Response System (Pan-STARRS; Chambers et al. 2016). For most (31 of 38) candidates, a counterpart was detected in *WISE* (Wright et al. 2010). Pan-STARRS host IDs and peak flare magnitudes

are listed in Table 1, and a color–magnitude diagram based on Pan-STARRS i and *WISE* W1 magnitudes is shown in Figure 3.

Of the 38 M dwarfs, three had spectra from the Sloan Digital Sky Survey (SDSS; SDSS Collaboration et al. 2017). For eight of the sources that were accessible in the night sky while this work was conducted, we obtained host spectra using the Double Spectrograph on the 200 inch Hale telescope at Palomar and the Low Resolution Imaging Spectrometer on Keck. These spectra are shown in Appendix B (in Figures 4 and 5, respectively).

In Table 1 we present derived properties of the flare stars. Note that this is not a complete sample of flaring M dwarfs in iPTF, because many were filtered out by the criterion of no prior or subsequent activity (criterion [c] in Section 2). To determine spectral type, we fit the spectra using the PyHammer software package (Kesseli et al. 2017). When a spectrum was not available, we used the quiescent Pan-STARRS colors and the relations in West et al. (2011) and Berger et al. (2013).

To estimate absolute magnitude, we used the relation between SDSS $r - z$ and M_r in Bochanski et al. (2011). More precisely, we interpolated between the values in Table 5 of that paper, assuming that the stars are active and have subsolar metallicity. Because some sources are outside the SDSS footprint, we used the $r - z$ color from Pan-STARRS instead. Using the sample in our work and in Berger et al. (2013), we find that in this magnitude range ($r = 16$–22 mag) the $r - z$ colors are equal to within 0.1 mag between SDSS and Pan-STARRS.

Note that the values in Table 1 are subject to large uncertainties. In general, M-dwarf classifications are only
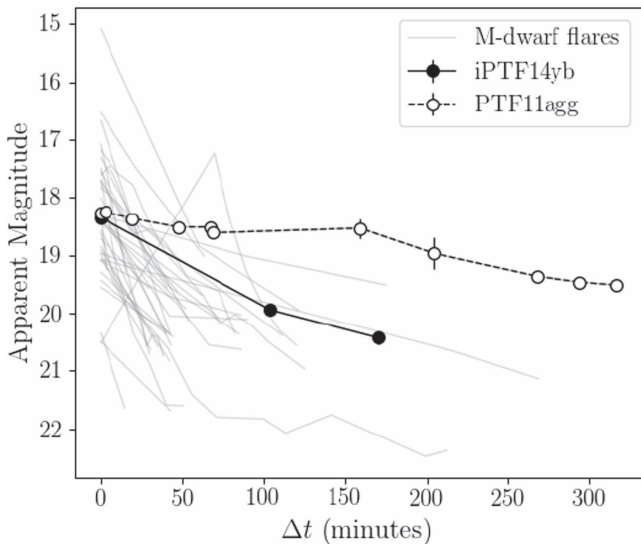
Figure 2. *r*-band light curves for the 38 M-dwarf flares in our sample (gray, background) overlaid with light curves of iPTF14yb and PTF11agg.
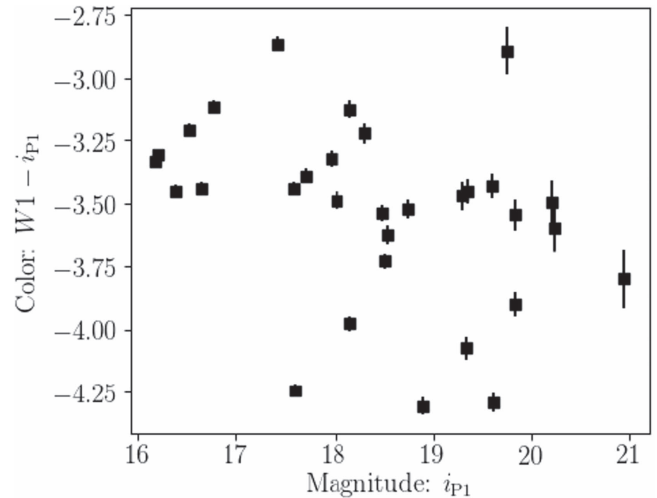

Figure 3. A color–magnitude diagram for 31 of the 38 M dwarfs in our sample using PanSTARRS *i* for the magnitude and *WISE* W1 − PanSTARRS *i* for the color. All of the M dwarfs have red counterparts in PanSTARRS, and most (31) have detected counterparts in *WISE*.

reliable to within one spectral type. Taking into account uncertainties in color, metallicity, and in the interpolation tables in Bochanski et al. (2011), the uncertainty in absolute magnitude M_r is roughly 25%. This translates into a factor of 3–4 uncertainty in distance d, a factor of 3–4 uncertainty in absolute height above the Galactic plane $|z|$, and an order of magnitude uncertainty in the peak luminosity of the flare $L_{\rm peak,flare}$. The u-band magnitude enhancement Δu is robust to uncertainties in spectral type to within 10%, and the percentile values are robust to uncertainties in spectral type to within 1%.

The fraction of active stars and the flare rate have been found to increase with later spectral type (Kowalski et al. 2009; West et al. 2011), so it is not surprising that most of the stars in our sample are spectral type M5 or M6. Furthermore, these stars are all located at small vertical distances from the Galactic plane, consistent with the finding in Kowalski et al. (2009) that flare rate decreases strongly with distance from the plane (stars lying close to the plane are younger, which may be associated with stronger activity).

Next, we compare the flare amplitudes to the sample in Kowalski et al. (2009) and list the percentile in the last column of Table 1. Kowalski et al. (2009) measured flare luminosities in the u-band.[19] To estimate the Δu of the flares in our sample, we convert Δr or Δg to Δu using the model in Davenport et al. (2012). The flares in our sample are large compared to those from most active stars of this spectral type. This is because of our selection criteria: the typical uncertainty on an iPTF magnitude is ~ 0.1, so a 5-σ change in magnitude is typically $\Delta r > 0.5$ or $\Delta g > 0.5$. A magnitude change of $\Delta r > 0.5$ corresponds to $\Delta u > 3$ in the Davenport et al. (2012) model, which is already at the 92nd percentile of the distribution in Kowalski et al. (2009).

4. Rate of Relativistic FOTs in iPTF

With iPTF14yb remaining the only confirmed afterglow in iPTF discovered independently of a high-energy trigger, we can constrain the rate of transients that exhibit the same fading behavior (peak at $m = 18$, fade by $\Delta m = 2$ mag in $\Delta t = 3$ hr). With our selection criteria and observations from 2013 February 1

through 2017 March 2, we follow a similar procedure to that in Section 5 of Cenko et al. (2015). We take all of the iPTF observations over this four-year period. We insert the light curve of iPTF14yb (for simplicity) stepping through a range of burst times. Using the limiting magnitude of the exposure and the brightness of the source at the time of observation, we determine whether or not the event would have been detected using our search criteria, i.e., two detections with a 5-σ difference in magnitude.

This gives a total areal exposure of $A_{\rm eff} = 22{,}146\ {\rm deg^2}$ days. So, we constrain the all-sky rate of on-axis relativistic transients similar to iPTF14yb to be

$$\mathcal{R} \equiv \frac{N_{\rm rel}}{A_{\rm eff}} = \frac{1}{22{,}146\ {\rm deg^2\ day}} \times \frac{365.25\ {\rm day}}{\rm year}$$
$$\times \frac{41{,}253\ {\rm deg^2}}{\rm sky} = 680\ {\rm yr^{-1}} \qquad (1)$$

with a 68% confidence interval from Poisson statistics of 119–2236 yr^{-1}. The expected rate of classical optical afterglows that can be detected by (i)PTF is two-thirds of the rate of on-axis *Swift* GRBs, or $\mathcal{R} = 970^{+53}_{-74}\ {\rm yr^{-1}}$ (Cenko et al. 2015). Thus, our search sets a limit on the relative rate of visible dirty fireballs to classical on-axis afterglows and suggests that it is, at most, comparable.

We now estimate the volumetric rate of transients with these characteristics (peak at $m = 18$, fade by $\Delta m = 2$ mag in $\Delta t = 3$ hr). iPTF14yb was observed at redshift $z = 1.9733 \pm 0.0003$ with spectral index $\beta = 1.3 \pm 0.1$ and apparent magnitude $m_{\rm p} = 18.16 \pm 0.03$ in its first discovery image. Applying a standard *K*-correction (Hogg et al. 2002), this corresponds to an absolute magnitude $M_{\rm p} = -27.5 \pm 0.1$ in the *r*-band some ~ 300 s after the initial outburst, which is fairly typical of the afterglows of *Swift* long GRBs (Cenko et al. 2009). Assuming iPTF14yb represents a population of standard candles (which is not really the case; see Kann et al. 2010), an identical explosion would appear with magnitude $m \approx 21$ if it occurred at redshift $z \approx 3$; thus we infer a volumetric rate of 0.395 Gpc^{-3} yr^{-1} with a 1σ credible interval of (0.022–0.708) Gpc^{-3} yr^{-1}. This is roughly consistent with one-third to two-thirds the rate of long-duration *Swift* GRBs in the

---

[19] M-dwarf flares are typically studied in the u-band because this holds the greatest contrast between the blue flare and red host.

Table 1
Host and Flare Properties of 38 iPTF FOTs Classified as M-dwarf Flares

iPTF ID	PS1 ID (PSO)	$m_{\mathrm{flare,iPTF}}$	Sp. Type	M	d	$|z|$	$L_{\mathrm{peak,flare}}$	Δu	Percentile	Notes
13agt	J170326.056+233048.207	20.8 ± 0.2	M6	14.0	790	8.0	5.6e+30	4.4	0.99	⋯
13asy	J122714.515+170827.218	20.4 ± 0.1	M5	12.0	810	19.0	8.8e+30	3.6	0.97	⋯
13bde	J163025.023+394425.607	20.1 ± 0.09	M4	11.0	980	13.0	1.7e+31	4.4	0.99	⋯
13bku	J132710.975+121305.263	20.1 ± 0.1	M5	10.0	2100	46.0	8e+31	4.1	0.98	⋯
13dqr	J022241.723+251722.567	21.1 ± 0.2	M5	13.0	730	7.4	3.6e+30	4.6	0.99	⋯
13gt	J133612.438+322415.839	20.03 ± 0.08	M5	11.0	1000	24.0	1.9e+31	3.4	0.97	⋯
13nn	J074457.731+522431.570	21.7 ± 0.2	M5	11.0	1400	13.0	8.7e+30	3.7	0.97	⋯
14q	J075205.876+464103.422	22.5 ± 0.2[†]	M3	9.7	1800	16.0	8.1e+30	6.0	1.0	⋯
15bgf	J204038.050+394012.906	20.3 ± 0.1	M4	11.0	1200	0.46	1.9e+31	4.6	0.99	⋯
15bm	J075629.265+195502.966	20.6 ± 0.1	M7	14.0	350	2.4	1.4e+30	5.8	1.0	⋯
15dto	J002938.210+034148.808	20.4 ± 0.2[†]	M5	12.0	560	10.0	5.7e+30	3.0	0.92	K
15ell	J034044.994+181735.258	19.56 ± 0.09	M5	12.0	1100	9.5	3.4e+31	4.6	0.99	K
16bse	J204045.160+411809.265	20.7 ± 0.2	M4	11.0	590	0.062	3.4e+30	4.6	0.99	P
16bxw	J002145.452+005843.242	19.5 ± 0.2	M6	12.0	180	3.4	9.9e+29	3.7	0.97	S, P
16ccd	J025954.415+602506.863	19.89 ± 0.08	M5	12.0	740	0.32	1.2e+31	3.3	0.94	K
17ady	J141130.672+304100.846	21.6 ± 0.1	M7	14.0	150	3.3	9.9e+28	3.8	0.97	⋯
17ahn	J164144.856+403623.379	20.3 ± 0.1	M5	10.0	1900	24.0	4.2e+31	5.0	0.99	K
17alz	J022942.051+191822.355	20.6 ± 0.1	M6	11.0	480	5.5	4e+30	5.3	0.99	P
17amj	J012608.197+353352.587	20.12 ± 0.09	M5	11.0	950	7.7	1.9e+31	4.0	0.98	K
17bub	J054206.049+700935.192	19.92 ± 0.09	M4	11.0	430	2.6	5.5e+30	3.3	0.94	⋯
17eur	J080132.966+180821.586	19.56 ± 0.08	M3	9.6	640	4.5	4.5e+30	4.2	0.98	⋯
17hce	J020737.876+135531.430	20.63 ± 0.09	M5	12.0	540	7.4	4.1e+30	5.1	0.99	⋯
17hhv	J072756.444+180748.975	20.3 ± 0.2	M4	11.0	280	1.4	3e+30	4.4	0.99	⋯
17hmf	J093025.725+114653.074	19.3 ± 0.1	M4	11.0	500	6.2	2e+30	6.3	1.0	⋯
17hmz	J080557.336+154053.582	21.0 ± 0.2	M5	13.0	240	1.7	6.8e+29	4.2	0.99	⋯
17ipt	J133442.745+055903.060	20.6 ± 0.2	M5	12.0	190	3.9	4.1e+29	4.1	0.98	⋯
17iwk	J153313.078+571537.332	20.6 ± 0.1	M4	10.0	360	5.4	1.8e+30	5.1	0.99	⋯
17jlt	J151344.316+200736.440	20.4 ± 0.1	M5	12.0	480	8.2	6.2e+30	4.6	0.99	⋯
17jq	J032221.653+264423.619	19.63 ± 0.09	M5	12.0	470	3.6	5.8e+30	3.8	0.97	⋯
17jqb	J150608.089+134859.802	19.7 ± 0.1	M5	13.0	620	11.0	8.2e+30	4.8	0.99	⋯
17jvl	J114254.502+275546.738	19.9 ± 0.1	M4	11.0	190	4.4	1.4e+30	4.7	0.99	⋯
17knl	J083105.765+160952.079	19.29 ± 0.07	M4	10.0	680	6.0	2.2e+31	5.0	0.99	⋯
17mlj	J074900.627+210136.013	19.0 ± 0.2	M4	11.0	220	1.5	1e+30	7.4	1.0	⋯
17py	J162922.139+335645.582	19.9 ± 0.2	M7	14.0	370	4.9	5.5e+30	3.5	0.97	⋯
17qfn	J103422.298+091040.949	19.24 ± 0.06	M4	11.0	610	9.9	3.8e+30	5.7	1.0	⋯
17rzn	J084115.859+181628.242	20.7 ± 0.1	M6	14.0	280	2.8	3.5e+29	6.4	1.0	S
17yz	J104639.306+323916.760	21.6 ± 0.2	M6	14.0	200	3.8	5.6e+29	6.2	1.0	S
17ze	J131505.985+430400.947	20.4 ± 0.1	M5	12.0	290	6.6	1.2e+30	5.1	0.99	

Note. iPTF mags with a † are in the g-band, otherwise in the r-band. In the notes section, K means a spectrum was obtained with LRIS on Keck, P means that a spectrum was obtained with the double spectrograph on the Palomar 200 inch telescope, S means that an SDSS spectrum was already available. Positions and spectra can be found in the supplementary material. As described in the text, M-dwarf classifications are only reliable to within one spectral type. Other uncertainties are roughly 25% in absolute magnitude M_r, a factor of 3–4 in distance d and absolute height above the galactic plane $|z|$, an order of magnitude in the peak luminosity of the flare $L_{\mathrm{peak,flare}}$, 10% in the u-magnitude Enhancement Δu, and 1% in the percentile of Δu.

local universe (1.3 Gpc^{-3} yr^{-1}; Wanderman & Piran 2010), without accounting for beaming. A more detailed analysis of this volumetric rate is forthcoming (A. Urban et al. 2018, in preparation).

5. Conclusions

The ZTF (Bellm & Kulkarni 2017) has just achieved first light, and with its 47 deg^2 field of view and faster readout it will represent, on average, a 12-fold increase in volumetric survey speed over PTF. Thus, in one routine semester of ZTF, we will be able to reproduce the coverage of iPTF, setting very strong limits on the rates of extragalactic FOTs, or potentially providing the first confirmed detection of afterglows lacking prompt high-energy emission.

So far, it seems that M-dwarf flares are the only astrophysical contaminant in searching for afterglows via rapidly fading emission. In particular, our selection criteria identify flares from late-type M dwarfs in the top decile of flare amplitude. Such

events are rare due to the intrinsic faintness of late-type M dwarfs and the anti-correlation of flare frequency with flare energy (e.g., Davenport 2016). Wide-area, high-cadence surveys such as PTF and ZTF are thus well-suited for identifying the most extreme examples of flaring activity (so-called "hyperflares"), aiding studies of chromospheric activity and stellar dynamos.

That said, the cadence of these wide-field surveys (PTF, ZTF, LSST) is not well-suited for constraining detailed physics of flares. Instead, the cadence is more suited to flare population statistics. The spatial distribution of these extreme examples of flaring activity is interesting because flares are typically an indicator of stellar youth. The same ZTF data (and other such surveys) can be used to measure rotation rates and therefore estimate stellar ages (gyrochronology). Therefore, properly modeling the transient contribution for flares could result in a relation between activity and rotation period for these stars. The latter is usually taken as a proxy for age.

It is a pleasure to thank Yi Cao, Jim Davenport, Adam Miller, Yuguang Chen, Harish Vendantham, Lynne Hillenbrand, and Trevor David for helpful discussions and assistance. We are grateful to the anonymous referee for constructive feedback that improved the quality of the paper. A.Y.Q.H. was supported by a National Science Foundation Graduate Research Fellowship under grant No. DGE1144469. D.A.K. acknowledges support from from the Spanish research project AYA 2014-58381-P and the Juan de la Cierva Incorporacíon fellowship IJCI-2015-261. This work was supported by the GROWTH project funded by the National Science Foundation under PIRE grant No. 1545949. The Intermediate Palomar Transient Factory project is a scientific collaboration among the California Institute of Technology, Los Alamos National Laboratory, the University of Wisconsin, Milwaukee, the Oskar Klein Center, the Weizmann Institute of Science, the TANGO Program of the University System of Taiwan, and the Kavli Institute for the Physics and Mathematics of the Universe. This research made use of Astropy, a community-developed core Python package for Astronomy (Astropy Collaboration et al. 2013).

Appendix A
Table of iPTF Fast Optical Transients

Table 2 contains the full list of fast optical transients found in our iPTF archival search. We provide their iPTF ID, position, discovery date, and classification.

Table 2
iPTF Fast Optical Transients

PTF ID	R.A.	Decl.	UT Date	Classification
13agt	17:03:26.07	+23:30:48.0	2013 Apr 04	M-dwarf
13asy	12:27:14.53	+17:08:27.2	2013 May 04	M-dwarf
13bde	16:30:25.03	+39:44:25.5	2013 May 15	M-dwarf
13bku	13:27:11.00	+12:13:05.2	2013 Jun 01	M-dwarf
13dqr	02:22:41.74	+25:17:22.6	2013 Oct 04	M-dwarf
13gt	13:36:12.43	+32:24:15.8	2013 Feb 18	M-dwarf
13nn	07:44:57.71	+52:24:31.4	2013 Mar 06	M-dwarf
13qz	12:02:07.82	+01:22:50.8	2013 Mar 13	Bad Subtraction
14cva	18:47:29.00	+49:43:51.7	2014 Jun 20	Afterglow
14cyb	15:01:53.41	+81:11:29.0	2014 Jun 23	Afterglow
14q	07:52:05.86	+46:41:03.2	2014 Jan 03	M-dwarf
14ts	10:05:47.69	+10:25:52.2	2014 Feb 22	Rock
14yb	14:45:58.01	+14:59:35.3	2014 Feb 26	Afterglow
15bgf	20:40:38.04	+39:40:12.7	2015 Jun 12	M-dwarf
15bm	07:56:29.27	+19:55:02.9	2015 Jan 18	M-dwarf
15dto	00:29:38.21	+03:41:48.9	2015 Nov 09	M-dwarf
15ell	03:40:45.01	+18:17:35.2	2015 Nov 20	M-dwarf
16bse	20:40:45.14	+41:18:08.9	2016 Jul 11	M-dwarf
16bxw	00:21:45.47	-00:58:43.1	2013 Oct 01	M-dwarf
16ccd	02:59:54.41	+60:25:06.7	2016 Nov 23	M-dwarf
16hdn	00:58:13.16	+06:24:00.9	2016 Oct 13	Bad Subtraction
17ady	14:11:30.65	+30:41:00.7	2013 Mar 15	M-dwarf
17ahn	16:41:44.86	+40:36:23.0	2013 May 21	M-dwarf
17alz	02:29:42.04	+19:18:22.5	2013 Sep 04	M-dwarf
17amj	01:26:08.20	+35:33:52.6	2013 Sep 07	M-dwarf
17bub	05:42:06.04	+70:09:35.1	2017 Mar 02	M-dwarf
17eur	08:01:32.94	+18:08:21.3	2014 Jan 07	M-dwarf
17hce	02:07:37.89	+13:55:31.5	2014 Nov 17	M-dwarf
17hhv	07:27:56.48	+18:07:49.0	2015 Jan 15	M-dwarf
17hmf	09:30:25.74	+11:46:53.1	2015 Feb 21	M-dwarf
17hmz	08:05:57.36	+15:40:54.2	2015 Mar 10	M-dwarf
17ipt	13:34:42.67	+05:59:02.4	2013 Mar 14	M-dwarf
17iwk	15:33:13.10	+57:15:36.8	2013 Apr 22	M-dwarf
17jlt	15:13:44.32	+20:07:36.6	2013 Mar 15	M-dwarf
17jq	03:22:21.67	+26:44:23.2	2014 Feb 11	M-dwarf
17jqb	15:06:08.11	+13:48:59.9	2013 Mar 15	M-dwarf
17jvl	11:42:54.48	+27:55:46.7	2013 Mar 14	M-dwarf
17knl	08:31:05.76	+16:09:51.7	2014 May 19	M-dwarf
17mlj	07:49:00.62	+21:01:35.7	2014 Jan 20	M-dwarf
17py	16:29:22.15	+33:56:45.5	2013 Mar 14	M-dwarf
17qfn	10:34:22.32	+09:10:40.9	2015 Feb 26	M-dwarf
17rzn	08:41:15.87	+18:16:28.0	2015 Jan 19	M-dwarf
17tq	04:57:50.59	+00:27:30.8	2013 Dec 14	Bad Subtraction
17ufp	08:01:27.39	+18:08:07.0	2015 Jan 19	Bad Subtraction
17uo	07:18:12.25	+64:21:19.6	2014 Jan 18	Bad Subtraction
17whs	01:54:27.77	+20:29:35.9	2013 Oct 05	Bad Subtraction
17wok	05:15:28.12	+01:30:47.1	2013 Dec 14	Bad Subtraction
17wsv	08:09:42.13	+19:45:05.3	2015 Jan 19	Bad Subtraction
17yz	10:46:39.27	+32:39:16.4	2013 Mar 11	M-dwarf
17ze	13:15:06.05	+43:04:01.5	2013 Mar 12	M-dwarf

Appendix B
Spectra of M-dwarf Hosts

Figures 4 and 5 show spectra of eight of the M dwarfs in our sample, obtained with the Double Spectrograph (DBSP) on the 200 inch Hale telescope at Palomar and the Low Resolution Imaging Spectrometer on Keck, respectively.
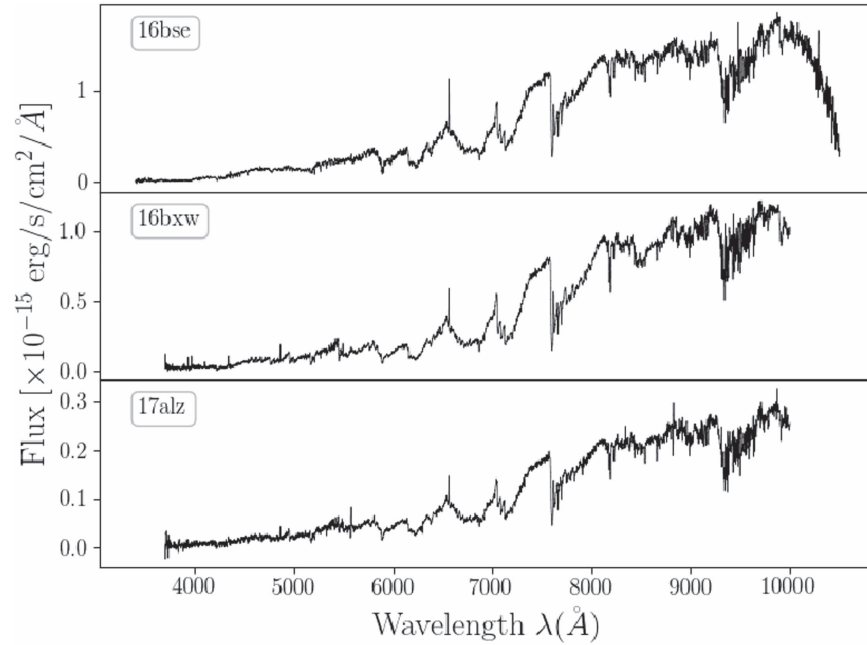

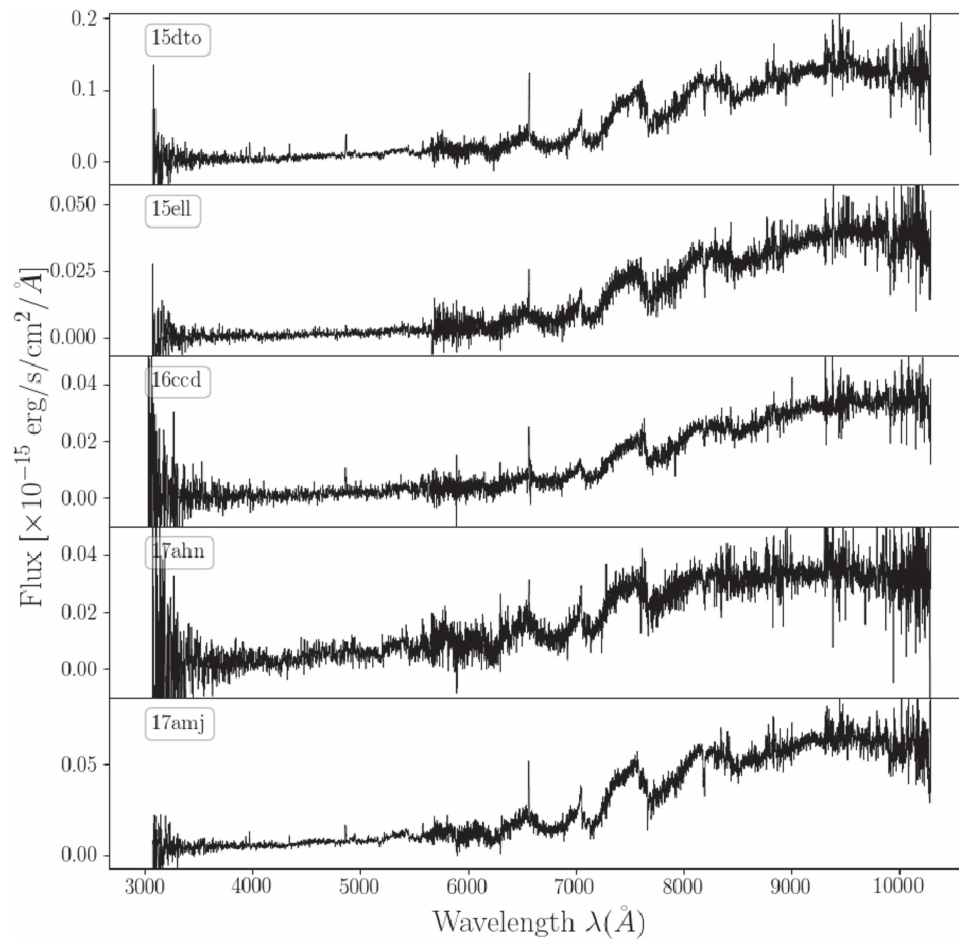**Figure 4.** DBSP spectra of three of the M dwarfs in our sample.

Figure 5. LRIS spectra of five of the M dwarfs in our sample.

ORCID iDs

Anna Y. Q. Ho ⓘ https://orcid.org/0000-0002-9017-3567
S. R. Kulkarni ⓘ https://orcid.org/0000-0001-5390-8563
Peter E. Nugent ⓘ https://orcid.org/0000-0002-3389-0586
S. Bradley Cenko ⓘ https://orcid.org/0000-0003-1673-970X
Vikram Ravi ⓘ https://orcid.org/0000-0002-7252-5485
Mansi M. Kasliwal ⓘ https://orcid.org/0000-0002-5619-4938
Daniel A. Perley ⓘ https://orcid.org/0000-0001-8472-1996
Christoffer Fremling ⓘ https://orcid.org/0000-0002-4223-103X
Avishay Gal-Yam ⓘ https://orcid.org/0000-0002-3653-5598
David Alexander Kann ⓘ https://orcid.org/0000-0003-2902-3583
David Kaplan ⓘ https://orcid.org/0000-0001-6295-2881
Frank Masci ⓘ https://orcid.org/0000-0002-8532-9395
Eran O. Ofek ⓘ https://orcid.org/0000-0002-6786-8774
Jesper Sollerman ⓘ https://orcid.org/0000-0003-1546-6615

References

Astropy Collaboration, Robitaille, T. P., Tollerud, E. J., et al. 2013, A&A, 558, A33
Bellm, E., & Kulkarni, S. 2017, NatAs, 1, 0071
Berger, E., Leibler, C. N., Chornock, R., et al. 2013, ApJ, 779, 18
Bhalerao, V., Kasliwal, M. M., Bhattacharya, D., et al. 2017, ApJ, 845, 152
Bloom, J. S., Richards, J. W., Nugent, P. E., et al. 2012, PASP, 124, 1175
Bochanski, J. J., Hawley, S. L., & West, A. A. 2011, AJ, 141, 98
Brink, H., Richards, J. W., Poznanski, D., et al. 2013, MNRAS, 435, 1047
Cao, Y., Nugent, P. E., & Kasliwal, M. M. 2016, PASP, 128, 114502
Cenko, S. B., Kelemen, J., Harrison, F. A., et al. 2009, ApJ, 693, 1484
Cenko, S. B., Kulkarni, S. R., Horesh, A., et al. 2013, ApJ, 769, 130
Cenko, S. B., Urban, A. L., Perley, D. A., et al. 2015, ApJL, 803, L24
Chambers, K. C., Magnier, E. A., Metcalfe, N., et al. 2016, arXiv:1612.05560
Davenport, J. R. A. 2016, ApJ, 829, 23
Davenport, J. R. A., Becker, A. C., Kowalski, A. F., et al. 2012, ApJ, 748, 58
Dermer, C. D., Chiang, J., & Mitman, K. E. 2000, ApJ, 537, 785
Drout, M. R., Chornock, R., Soderberg, A. M., et al. 2014, ApJ, 794, 23
Ghirlanda, G., Salvaterra, R., Campana, S., et al. 2015, A&A, 578, A71
Hogg, D. W., Baldry, I. K., Blanton, M. R., & Eisenstein, D. J. 2002, arXiv:astro-ph/0210394
Kann, D. A., Klose, S., Zhang, B., et al. 2010, ApJ, 720, 1513
Kasliwal, M. M., Cenko, S. B., & Singer, L. P. 2014, GCN, 16425
Kesseli, A. Y., West, A. A., Veyette, M., et al. 2017, ApJS, 230, 16
Kowalski, A. F., Hawley, S. L., Hilton, E. J., et al. 2009, AJ, 138, 633
Kulkarni, S. R., & Rau, A. 2006, ApJL, 644, L63
Law, N. M., Kulkarni, S. R., Dekany, R. G., et al. 2009, PASP, 121, 1395
Masci, F. J., Laher, R. R., Rebbapragada, U. D., et al. 2017, PASP, 129, 014002
Nakar, E., Piran, T., & Granot, J. 2002, ApJ, 579, 699
Piran, T. 2004, RvMP, 76, 1143
Rau, A., Ofek, E. O., Kulkarni, S. R., et al. 2008, ApJ, 682, 1205
Rhoads, J. E. 1997, ApJL, 487, L1
Rhoads, J. E. 2003, ApJ, 591, 1097
Singer, L. P., Kasliwal, M. M., Cenko, S. B., et al. 2015, ApJ, 806, 52
SDSS Collaboration, Albareti, F. D., Allende Prieto, C., et al. 2017, ApJS, 233, 25
Stalder, B., Tonry, J., Smartt, S. J., et al. 2017, ApJ, 850, 149
von Kienlin, A. 2014, GCN, 16450
Wanderman, D., & Piran, T. 2010, MNRAS, 406, 1944
West, A. A., Morgan, D. P., Bochanski, J. J., et al. 2011, AJ, 141, 97
Wright, E. L., Eisenhardt, P. R. M., Mainzer, A. K., et al. 2010, AJ, 140, 1868
Yang, S., Valenti, S., Cappellaro, E., et al. 2017, ApJL, 851, L48